Ni doped Co-MOF-74 synergized with 2D $Ti_3C_2T_x$ MXene as an efficient electrocatalyst for overall water-splitting

Ke Yu, Jingyuan Zhang, Yuting Hu, Lanqi Wang, Xiaofeng Zhang, Bin Zhao*

School of Materials & Chemistry, University of Shanghai for Science and Technology, Shanghai 200093, China
* Correspondence: zhaobin@usst.edu.cn

Supporting information

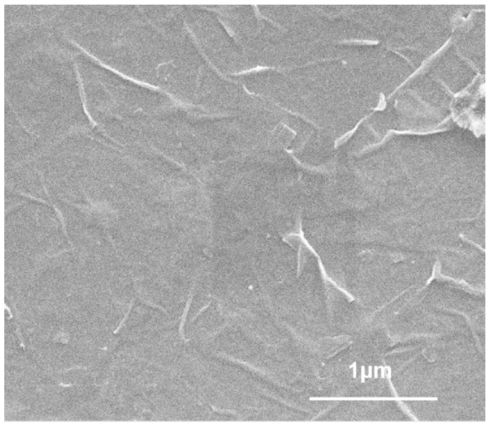

Figure S1. SEM image of as-prepared few-layer $Ti_3C_2T_x$ MXene.

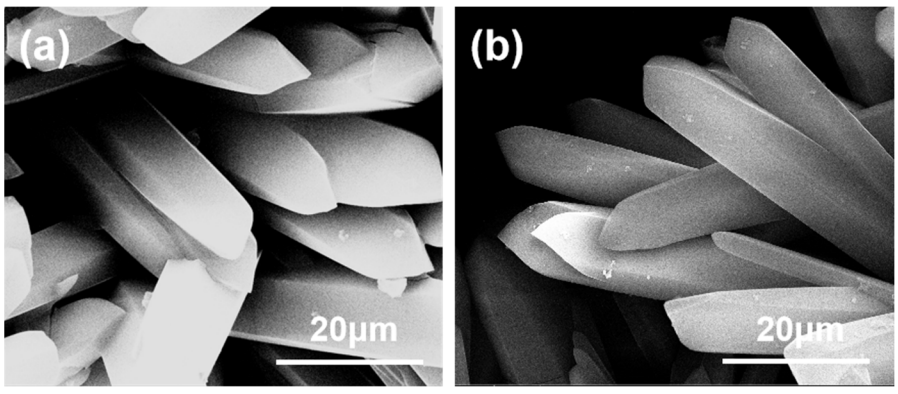

Figure S2. SEM images of a) $CoNi_{0.1}$-MOF-74/MXene/NF, b)$CoNi_{0.03}$-MOF-74/MXene/NF.

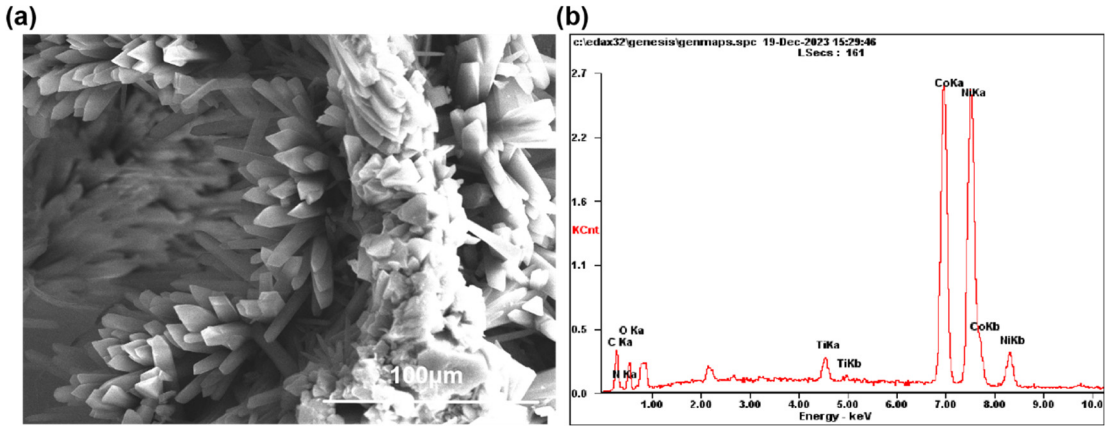

Figure S3. The SEM (a) and corresponding EDS spectra (b) of $CoNi_{0.04}$-MOF-74/MXene.

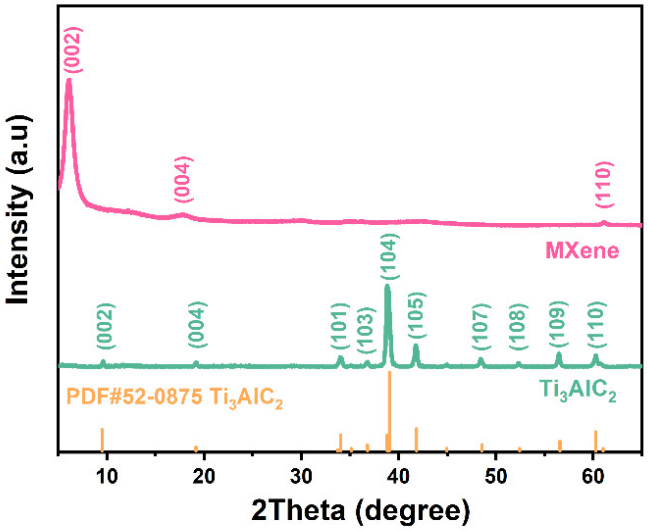

Figure S4. XRD patterns of MXene and Ti_3AlC_2

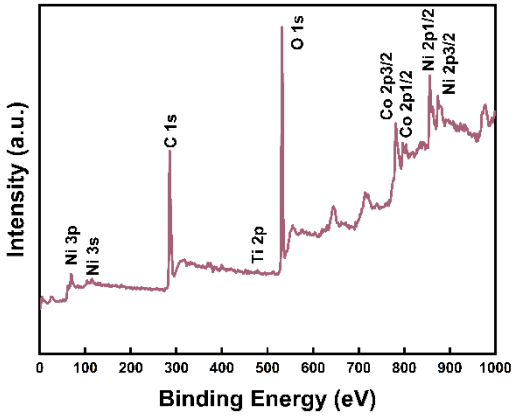

Figure S5. XPS survey spectra of $CoNi_{0.04}$-MOF-74/MXene/NF.

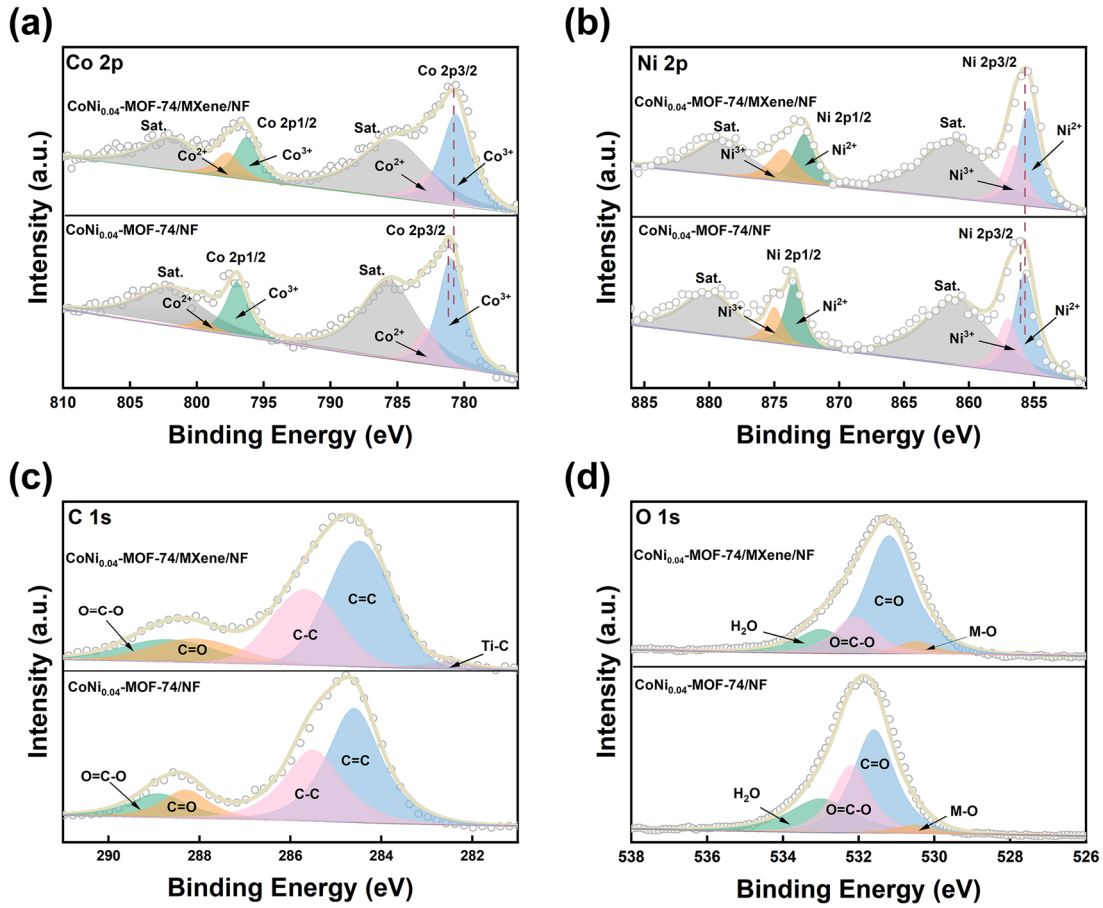

Figure S6. XPS (a) Co 2p, (b) Ti 2p, (c) C 1s, and (d) O 1s spectra of the $CoNi_{0.04}$-MOF-74/MXene/NF and $CoNi_{0.04}$-MOF-74/NF.

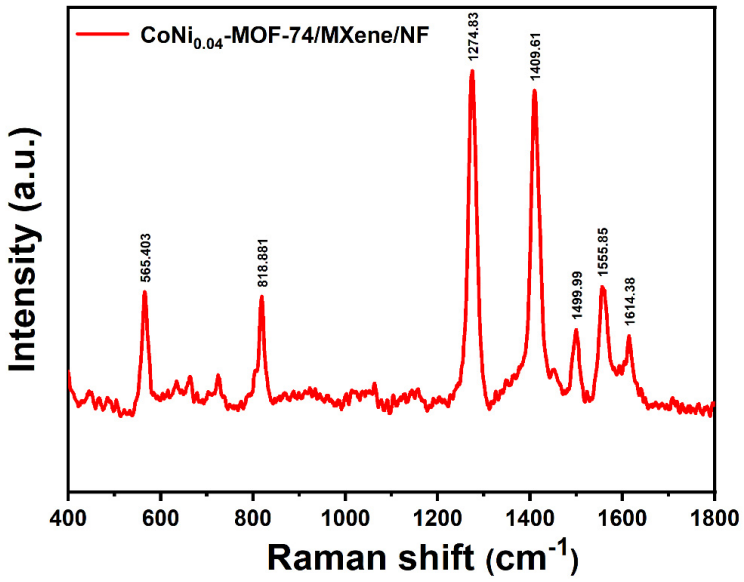

Figure S7. Raman spectra of $CoNi_{0.04}$-MOF-74/MXene/NF

The TOF value was calculated based on the following equation:

$$TOF = JA/(4Fm)$$

in which TOF is based on the number of redox-active sites, J is the current density at a specific overpotential, A is the area of the electrode, F is the Faraday constant, and m is the number of active sites.

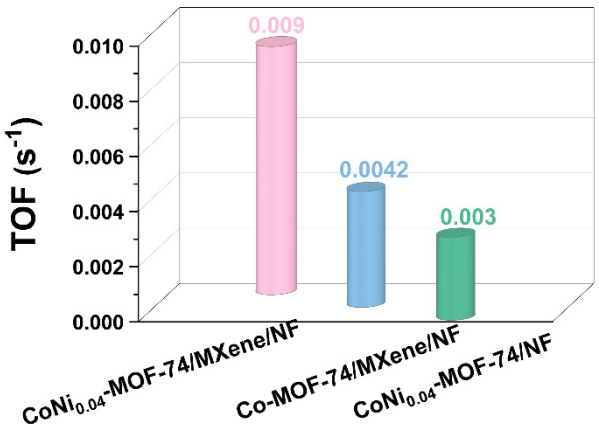

Figure S8. TOF of the $CoNi_{0.04}$-MOF-74/MXene/NF, Co-MOF-74/MXene/NF and $CoNi_{0.04}$-MOF-74/NF for OER.

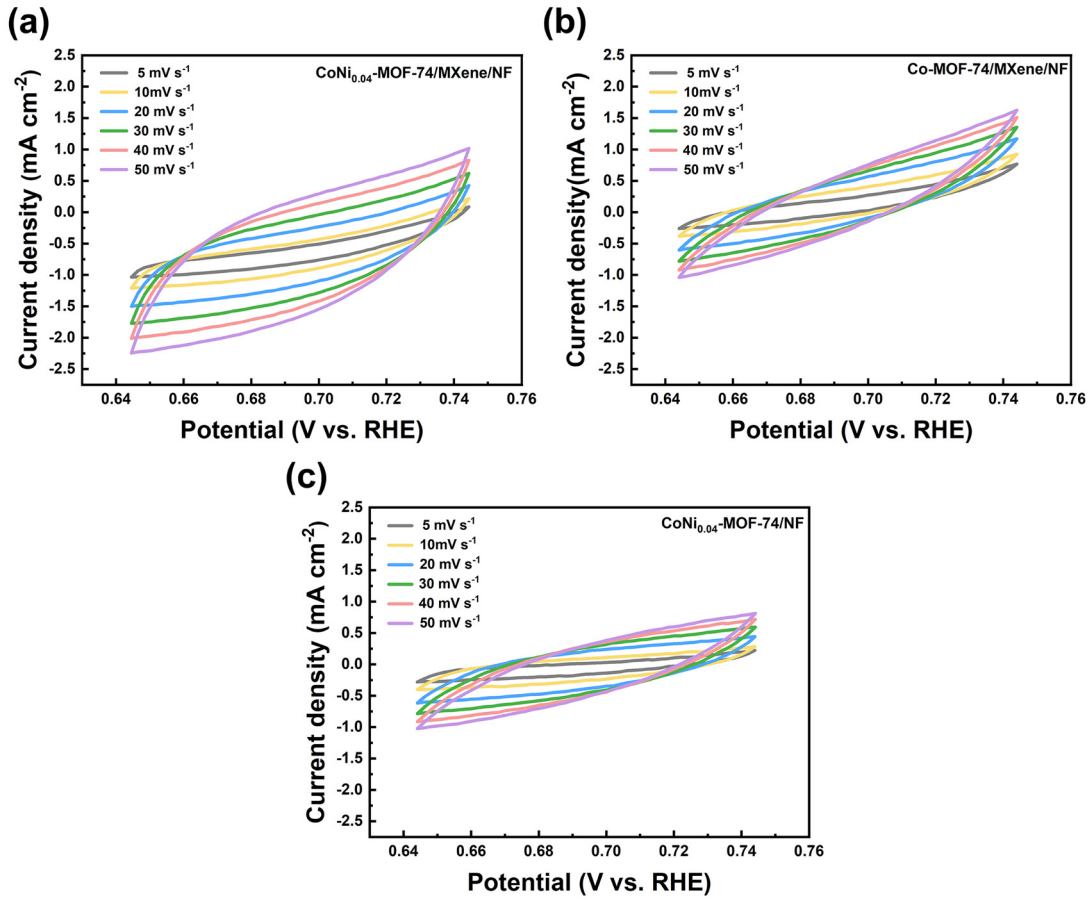

Figure S9. CV curves of the CoNi$_{0.04}$-MOF-74/MXene/NF (a), Co-MOF-74/MXene/NF (b), CoNi$_{0.04}$-MOF-74/NF (c) under different scan rates in the region of 0.644 - 0.744 V vs. RHE for OER process.

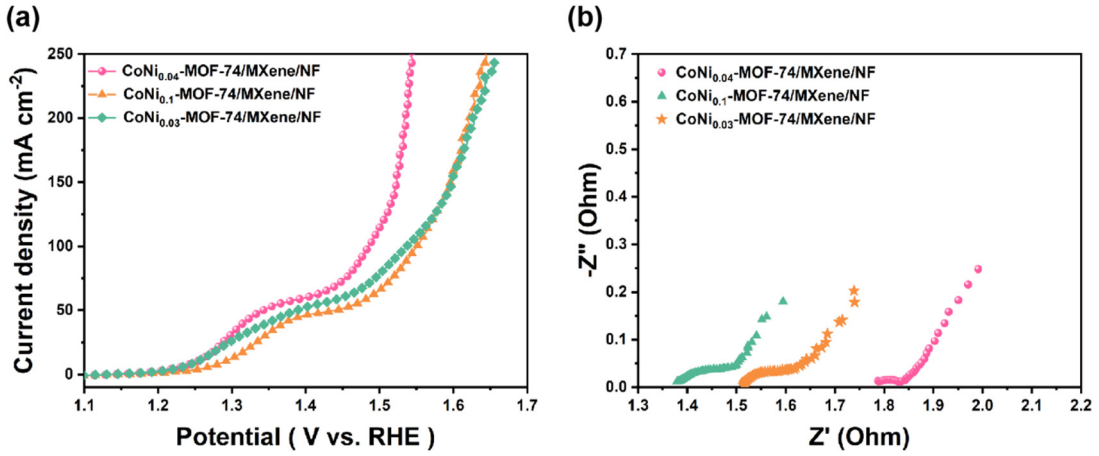

Figure S10. (a) OER polarization curves and (b) Nyquist plots of CoNi$_{0.1}$-MOF-74/MXene/NF, CoNi$_{0.04}$-MOF-74/MXene/NF, CoNi$_{0.03}$-MOF-74/MXene/NF.

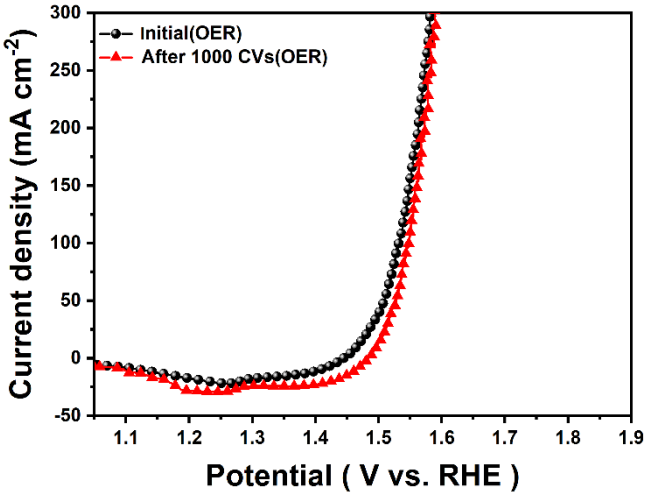

Figure S11. OER polarization curves for $CoNi_{0.04}$-MOF-74/MXene/NF before and after 1,000 cycles.

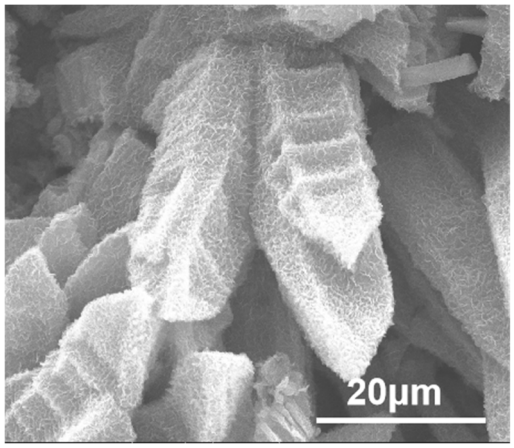

Figure S12. SEM images of $CoNi_{0.04}$-MOF-74/MXene/NF after OER test.

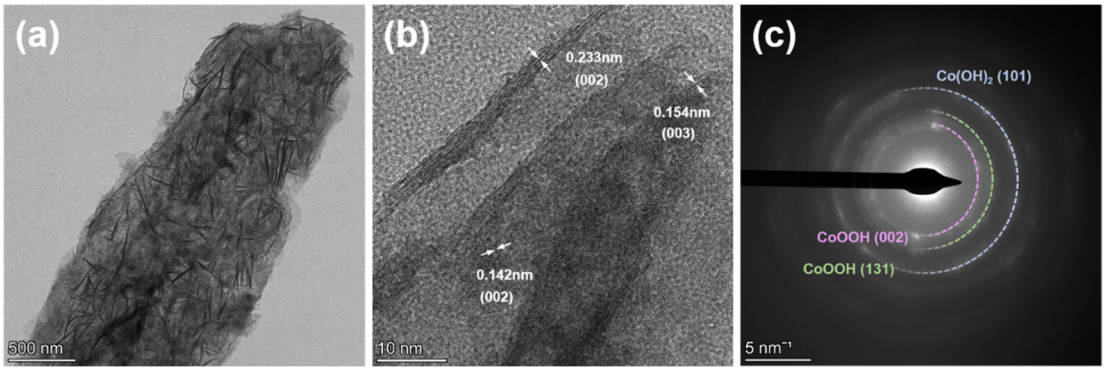

Figure S13. TEM images of (a) $CoNi_{0.04}$-MOF-74/MXene/NF after the OER test; HRTEM image (b) and SAED patterns (c) of $CoNi_{0.04}$-MOF-74/MXene/NF after the OER test.

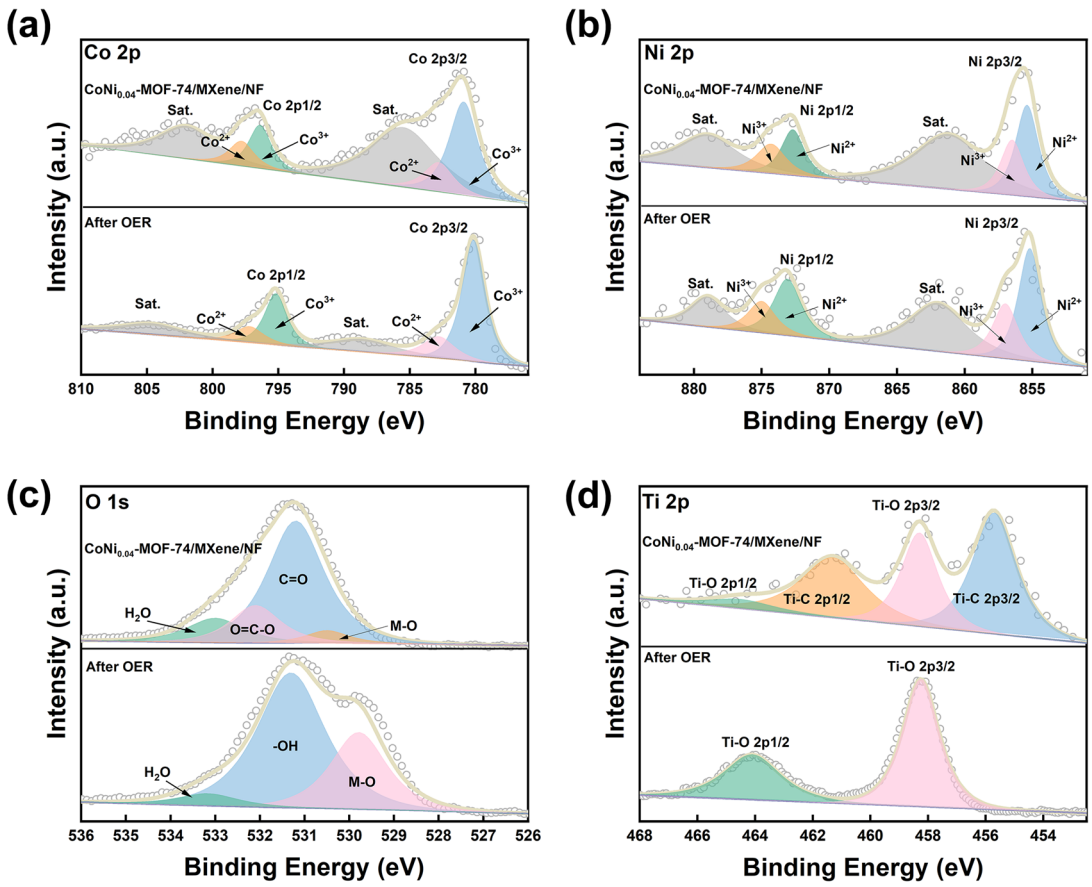

Figure S14. XPS (a) Co 2p, (b) Ni 2p, (c) O 1s, and (d) Ti 2p spectra of the $CoNi_{0.04}$-MOF-74/MXene/NF and XPS spectra of $CoNi_{0.04}$-MOF-74 /MXene/NF after the OER test.

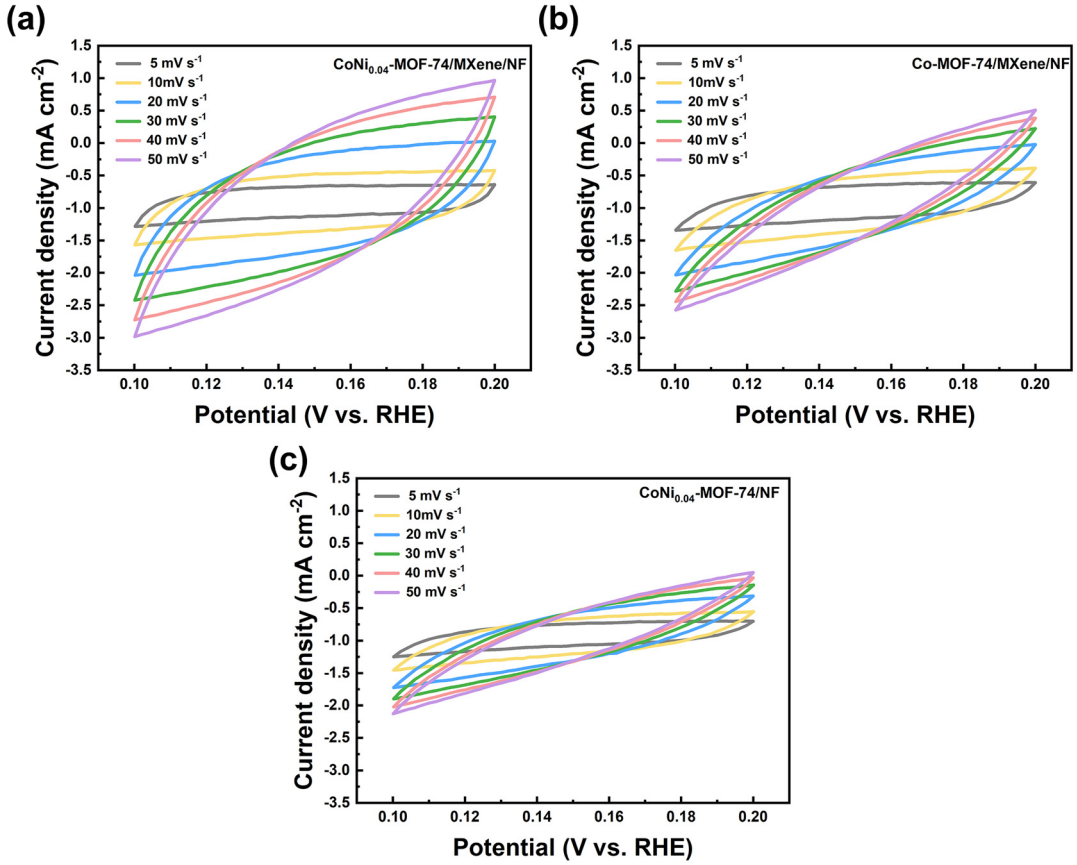

Figure S15. CV curves of the CoNi$_{0.04}$-MOF-74/MXene/NF (a), Co-MOF-74/MXene/NF (b), CoNi$_{0.04}$-MOF-74/NF (c) under different scan rates in the region of 0.1 - 0.2 V vs. RHE for HER process.

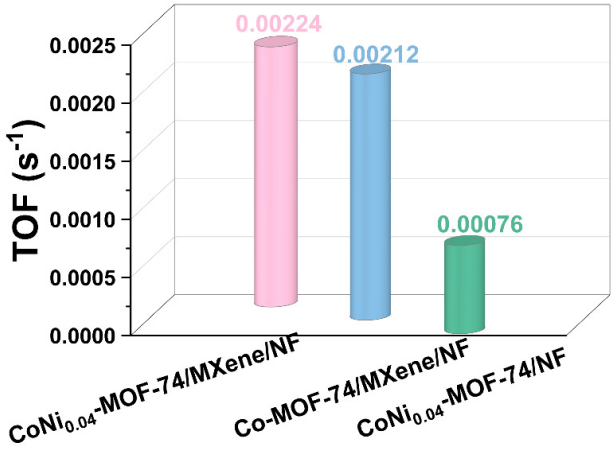

Figure S16. TOF of the CoNi$_{0.04}$-MOF-74/MXene/NF, Co-MOF-74/MXene/NF and CoNi$_{0.04}$-MOF-74/NF for HER.

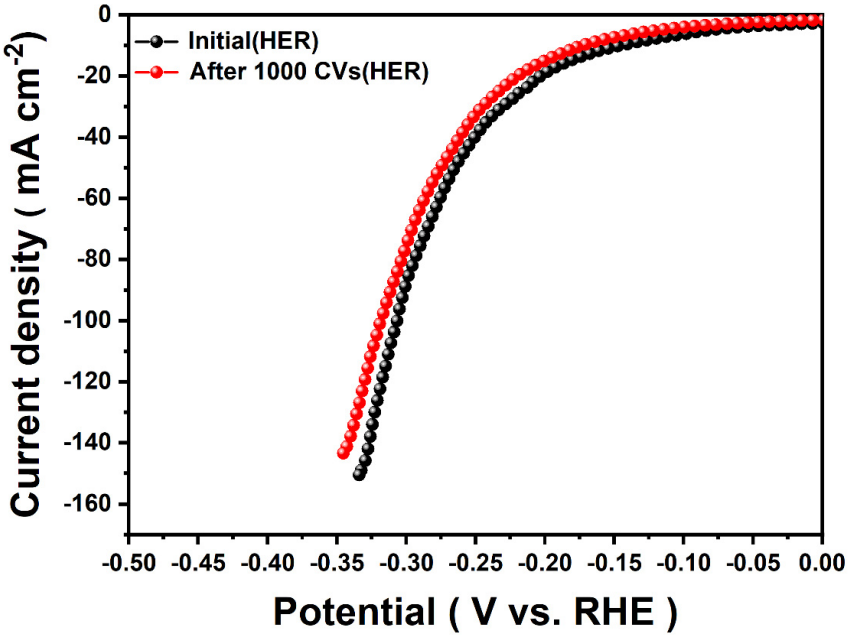

Figure S17. HER polarization curves for $CoNi_{0.04}$-MOF-74/MXene/NF before and after 1,000 cycles.

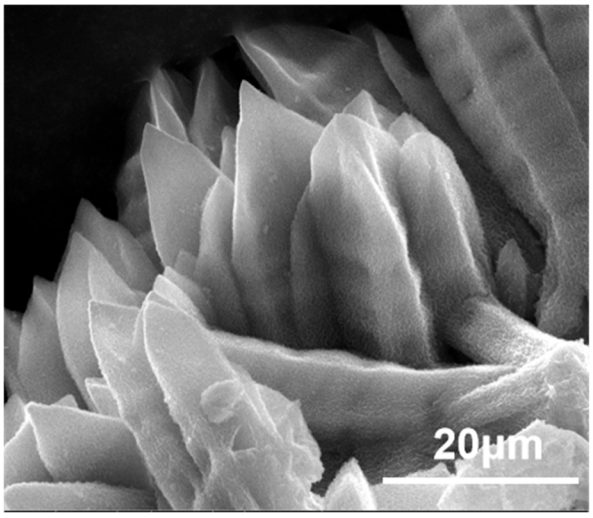

Figure S18. SEM images of $CoNi_{0.04}$-MOF-74/MXene/NF after HER test.

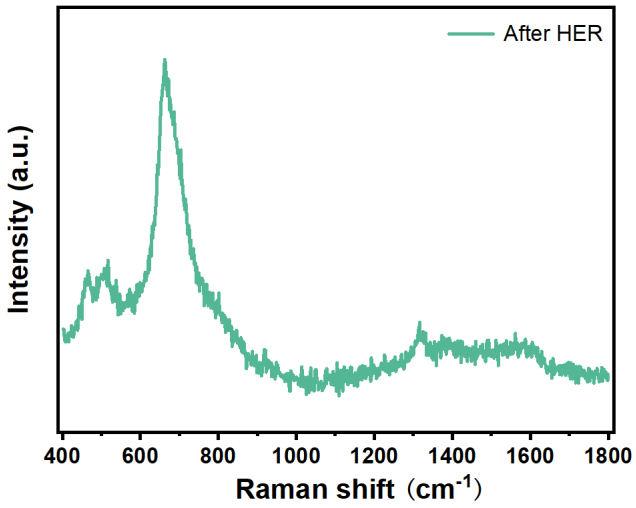

Figure S19. Raman spectra of $CoNi_{0.04}$-MOF-74/MXene/NF after the HER test.

Table S1. Co2p peak area ratio of $CoNi_{0.04}$-MOF-74/MXene/NF and Co-MOF-74/MXene/NF calculated from XPS spectra.

	$CoNi_{0.04}$-MOF-74/MXene/NF	Co-MOF-74/MXene/NF
Co^{2+}	12.7%	19.9%
Co^{3+}	31.7%	28.7%

Table S2. Comparison of Electrochemical performances of OER of $CoNi_{0.04}$-MOF-74/MXene/NF with recently reported OER electrocatalysts in 1 M KOH.

Materials	Overpotential (mV)	Tafel slope (mV dec $^{-1}$)	References
$CoNi_{0.04}$-MOF-74/MXene/NF	256(η100)	46.7	Our Work
Co_2Ni-MOF@MX-1	265(η10)	51.7	[1]
Ti_2NT_x@MOF-CoP	241(η50)	65.8	[2]
MX@MOF-Co_2P	246(η10)	39.29	[3]
Ti_3C_2@mNiCoP	237(η10)	104	[4]
$Ni_{0.7}Fe_{0.3}PS_3$@MXene	282(η10)	36.5	[5]
Mo–NiCoP@MXene/NF	280(η10)	56.91	[6]
Ru@NiCo-MOF HPNs	284(η10)	78.8	[7]
CoNi MOF-CNTs	306 (η10)	42	[8]

Table S3. OER catalyst EIS fitting parameters.

Materials	Rs(Ω)	Rct(Ω)	CPE(Ω)
$CoNi_{0.04}$-MOF-74/MXene	1.77	0.109	0.53
Co-MOF-74/MXene	1.48	0.37	0.56
$CoNi_{0.04}$-MOF-74/NF	1.669	1.38	0.51
MXene/NF	1.738	58.61	0.72

Table S4. Area ratios of Co2p and Ni2p peaks calculated from XPS spectra for $CoNi_{0.04}$-MOF-74/MXene/NF and after OER testing.

	$CoNi_{0.04}$-MOF-74/MXene/NF	After OER
Co^{2+}	12.7%	16.9%
Co^{3+}	31.7%	61.2%
Ni^{2+}	28.5%	40.7%
Ni^{3+}	9.7%	22.0%

Table S5. HER catalyst EIS fitting parameters.

Materials	Rs(Ω)	Rct(Ω)	CPE(Ω)
$CoNi_{0.04}$-MOF-74/MXene	1.687	8.518	0.72
Co-MOF-74/MXene	2.299	12.2	0.69
$CoNi_{0.04}$-MOF-74/NF	1.619	33.69	0.72
MXene/NF	1.662	72.43	0.74

Table S6. Comparison of Electrochemical performances of OWS of $CoNi_{0.04}$-MOF-74/MXene/NF with recently reported OWS electrocatalysts in 1 M KOH.

Catalyst	Cell voltage [V] at 10 mA cm^{-2}	References
$CoNi_{0.04}$-MOF-74/MXene/NF	1.49	Our Work
Ti_2NT_x@MOF-CoP	1.61	[2]
CdFe-BDC	1.64	[9]
CoNiBDC/CC	1.625	[10]
Ni-ZIF/Ni-B@NF	1.54	[11]
Fe_2Ni-MIL-88B/NFF	1.56	[12]
NiFe-MOF-74	1.58	[13]
NiFe-MOF	1.57	[14]
$FeMn_6Ce_{0.5}$-MOF-74/NF	1.65	[15]

References

1. Tan, P.; Gao, R.; Zhang, Y.; Han, N.; Jiang, Y.; Xu, M.; Bao, S.-J.; Zhang, X. Electrostatically directed assembly of two-dimensional ultrathin Co_2Ni-MOF/$Ti_3C_2T_x$ nanosheets for electrocatalytic oxygen evolution. *J. Colloid Interface Sci.* 2023, *630*, 363–371. https://doi.org/https://doi.org/10.1016/j.jcis.2022.10.109
2. Zong, H.; Qi, R.; Yu, K.; Zhu, Z. Ultrathin Ti_2NT_x MXene-wrapped MOF-derived CoP frameworks towards hydrogen evolution and water oxidation. *Electrochim. Acta* 2021, *393*, 139068. https://doi.org/https://doi.org/10.1016/j.electacta.2021.139068.
3. Li, J.; Chen, C.; Lv, Z.; Ma, W.; Wang, M.; Li, Q.; Dang, J. Constructing heterostructures of ZIF-67 derived C, N doped Co_2P and $Ti_2VC_2T_x$ MXene for enhanced OER. *J. Mater. Sci. Technol.* 2023, *145*, 74–82. https://doi.org/https://doi.org/10.1016/j.jmst.2022.10.048
4. Yue, Q.; Sun, J.; Chen, S.; Zhou, Y.; Li, H.; Chen, Y.; Zhang, R.; Wei, G.; Kang, Y. Hierarchical Mesoporous MXene–NiCoP Electrocatalyst for Water-Splitting. *ACS Appl. Mater. Interfaces* 2020, *12*, 18570–18577. https://doi.org/10.1021/acsami.0c01303.
5. Du, C.-F.; Dinh, K.N.; Liang, Q.; Zheng, Y.; Luo, Y.; Zhang, J.; Yan, Q. Self-Assemble and In Situ Formation of $Ni_{1-x}Fe_xPS_3$ Nanomosaic-Decorated MXene Hybrids for Overall Water Splitting. *Adv. Energy Mater.* 2018, *8*, 1801127. https://doi.org/https://doi.org/10.1002/aenm.201801127.
6. Jiang, J.; Sun, R.; Huang, X.; Xu, W.; Zhou, S.; Wei, Y.; Han, S.; Li, Y. In-situ derived Mo-doped NiCoP and MXene to form Mott-Schottky heterojunction with tunable surface electron density to promote overall water splitting. *Compos. Part B Eng.* 2023, *263*, 110834. https://doi.org/https://doi.org/10.1016/j.compositesb.2023.110834.
7. Liu, D.; Xu, H.; Wang, C.; Shang, H.; Yu, R.; Wang, Y.; Li, J.; Li, X.; Du, Y. 3D Porous Ru-Doped NiCo-MOF Hollow Nanospheres for Boosting Oxygen Evolution Reaction Electrocatalysis. *Inorg. Chem.* 2021, *60*, 5882–5889. https://doi.org/10.1021/acs.inorgchem.1c00295.
8. Yu, S.; Wu, Y.; Xue, Q.; Zhu, J.-J.; Zhou, Y. A novel multi-walled carbon nanotube-coupled CoNi MOF composite enhances the oxygen evolution reaction through synergistic effects. *J. Mater. Chem. A* 2022, *10*, 4936–4943. https://doi.org/10.1039/D1TA10681C.
9. Luo**, Y.;** Yang, **X.;** He, **L.;** Zheng, Y.**;** Pang, J.**;** Wang, L.**;** Jiang, R.**;** Hou, J.**;** Guo, X.**;** Chen, L. Structural and Electronic Modulation of Iron-Based Bimetallic Metal–Organic Framework Bifunctional Electrocatalysts for Efficient Overall Water Splitting in Alkaline and Seawater Environment, *ACS Appl. Mater. Interfaces* 2022**, *14*,** 46374–46385. https://doi.org/10.1021/acsami.2c05181.
10. Bai, X.-J.; Chen, H.; Li, Y.-N.; Shao, L.; Ma, J.-C.; Li, L.-L.; Chen, J.-Y.; Wang, T.-Q.; Zhang, X.-M.; Zhang, L.-Y.; et al. CoNi-based metal–organic framework nanoarrays supported on carbon cloth as bifunctional electrocatalysts for efficient water-splitting. *New J. Chem.* 2020, *44*, 1694–1698. https://doi.org/10.1039/C9NJ06204A.
11. Xu, H.; Fei, B.; Cai, G.; Ha, Y.; Liu, J.; Jia, H.; Zhang, J.; Liu, M.; Wu, R. Boronization-Induced Ultrathin 2D Nanosheets with Abundant Crystalline–Amorphous Phase Boundary Supported on Nickel Foam toward Efficient Water Splitting. *Adv. Energy Mater.* 2020, *10*, 1902714. https://doi.org/https://doi.org/10.1002/aenm.201902714.
12. Raja, D.S.; Chuah, X.-F.; Lu, S.-Y. In Situ Grown Bimetallic MOF-Based Composite as Highly Efficient Bifunctional Electrocatalyst for Overall Water Splitting with Ultrastability at High Current Densities. *Adv. Energy Mater.* 2018, *8*, 1801065. https://doi.org/https://doi.org/10.1002/aenm.201801065.
13. Chen, C.; Suo, N.; Han, X.; He, X.; Dou, Z.; Lin, Z.; Cui, L. Tuning the morphology and electron structure of metal-organic framework-74 as bifunctional electrocatalyst for OER and HER using bimetallic collaboration strategy. *J. Alloys Compd.* 2021, *865*, 158795. https://doi.org/https://doi.org/10.1016/j.jallcom.2021.158795.
14. Mou, Q.; Xu, Z.; Wang, G.; Li, E.; Liu, J.; Zhao, P.; Liu, X.; Li, H.; Cheng, G. A bimetal hierarchical layer structure MOF grown on Ni foam as a bifunctional catalyst for the OER and HER. *Inorg. Chem. Front.* 2021, *8*, 2889–2899. https://doi.org/10.1039/D1QI00267H.
15. Chai, N.; Kong, Y.; Liu, T.; Ying, S.; Jiang, Q.; Yi, F.-Y. (FeMnCe)-co-doped MOF-74 with significantly improved performance for overall water splitting. *Dalton Trans.* 2023, *52*, 11601–11610. https://doi.org/10.1039/D3DT01892J.